

# Magnetic Nanocomposite Hydrogels for Directing Myofibroblast Activity in Adipose-Derived Stem Cells

Md Shariful Islam, Thomas G. Molley, Jake Ireland, Jamie J. Kruzic, and Kristopher A. Kilian\*

Dynamic cell-culture materials that can change mechanical properties in response to extrinsic stimuli are emerging as promising tools for cell and tissue engineering research. However, most of these techniques involve a one-way stiffening or softening through changes in the materials chemistry, which does not allow reversibility. Here, the incorporation of superparamagnetic iron-oxide nanoparticles within poly(ethylene glycol) hydrogels as dynamic cell culture materials is demonstrated. Using simple permanent magnets and adipose-derived stem cells, a near twofold increase in cell spread area and an accompanying 20% enrichment in cells expressing alpha-smooth muscle actin is seen. This platform provides a means to study relationships between dynamic stiffening and cell behavior, using permanent magnets and clinically viable composite materials, with scope for use as a tool to enrich the myofibroblast population in stromal cells.


## 1. Introduction

Intrinsic and extrinsic mechanical forces influence the growth, morphogenesis, and differentiation of cells during development.<sup>[1]</sup> As development progresses, interactions between cells and the extracellular matrix (ECM) guide lineage determination by transmitting forces from cell-matrix engagement through focal

M. S. Islam, T. G. Molley, Prof. K. A. Kilian  
School of Materials Science and Engineering  
The University of New South Wales  
Sydney, NSW 2052, Australia  
E-mail: k.kilian@unsw.edu.au

J. Ireland, Prof. K. A. Kilian  
School of Chemistry  
Australian Centre for Nanomedicine  
The University of New South Wales  
Sydney, NSW 2052, Australia

Prof. J. J. Kruzic  
School of Mechanical and Manufacturing Engineering  
The University of New South Wales  
Sydney, NSW 2052, Australia

 The ORCID identification number(s) for the author(s) of this article can be found under <https://doi.org/10.1002/anbr.202000072>.

© 2021 The Authors. Advanced NanoBiomed Research published by Wiley-VCH GmbH. This is an open access article under the terms of the Creative Commons Attribution License, which permits use, distribution and reproduction in any medium, provided the original work is properly cited.

DOI: 10.1002/anbr.202000072

adhesions, into the cytoplasm, and to the nuclear membrane to directly and indirectly dictate gene expression programs.<sup>[2–4]</sup> Researchers have developed a host of dynamic synthetic materials with controllable properties to study how matrix mechanics influence cell behavior.<sup>[5]</sup> The stiffness of engineered ECM materials have been modulated through either crosslinking density<sup>[6,7]</sup> or using external stimuli such as light,<sup>[8]</sup> temperature,<sup>[9]</sup> pH,<sup>[10]</sup> ionic additives,<sup>[11]</sup> ultrasound<sup>[12]</sup> and magnetic force.<sup>[13]</sup> Although these approaches have shown great success in changing matrix properties as well as influencing cell activity, complex chemical modification are invariably necessary, which obviates the ease of translation to diverse laboratory settings.

Cell size and morphology are influenced by matrix stiffness.<sup>[14–16]</sup> On a stiff surface, cells can adopt robust focal adhesions with an organized cytoskeleton, thereby facilitating a dynamic push and pull, whereas on soft surface, cells fail to develop this contractile network. In addition to cell morphology, stiffness also influences cellular functions such a proliferation<sup>[17–19]</sup> and differentiation.<sup>[20–22]</sup> An important contractile cell type for tissue engineering is the myofibroblast, which will show diverse adhesive characteristics on stiff and soft substratum.<sup>[23,24]</sup> Human mesenchymal stem cells (MSCs) are a promising cell source for vascular tissue engineering, as these fibroblastic stromal cells readily express smooth-muscle actin and can undergo myofibroblast differentiation.<sup>[25]</sup> MSC lineage specification can be influenced by biochemical and biophysical properties such as substrate stiffness,<sup>[26,27]</sup> cell geometry,<sup>[28,29]</sup> and matrix protein composition.<sup>[30,31]</sup> Furthermore, MSCs show multiple differentiation capacities such as differentiating into myofibroblasts via direct treatment with soluble factors<sup>[32,33]</sup> or by mechanical stimulation of the substrate.<sup>[34,35]</sup>

In this article, we present a simple approach to influence myofibroblast differentiation by incorporating magnetic nanoparticles into hydrogels, where attenuation of a magnetic field leads to substrate stiffening. Nanoscale Fe<sub>3</sub>O<sub>4</sub> was fabricated through a chemical coprecipitation method and polymerized directly within poly(ethylene glycol) dimethacrylate (PEGDM) hydrogels. The physicochemical properties of the nanoparticles and the hydrogel network architecture enabled particle retention within the material. Average cell area changes with the presence of a magnetic field leads to an increase in the fraction of cultured MSCs displaying a myofibroblast phenotype.

## 2. Experimental Section

### 2.1. Synthesis and Characterization of Fe<sub>3</sub>O<sub>4</sub> Nanoparticles

Fe<sub>3</sub>O<sub>4</sub> nanoparticles were synthesized with a chemical coprecipitation method by reacting iron salts with ammonium hydroxide solution in a nitrogen environment as previously reported.<sup>[36,37]</sup> Briefly, 0.2 M FeCl<sub>3</sub>·6H<sub>2</sub>O and 0.1 M FeCl<sub>2</sub>·4H<sub>2</sub>O (Bio-Strategy Pty Ltd.) were dissolved in deionized water under a nitrogen gas flow. The salt mixtures were added dropwise over the course of 5 min to 0.8 M NH<sub>4</sub>OH (Sigma-Aldrich Pty Ltd.) solution with vigorous stirring in room temperature and at pH = 11–12. Formations of instant black precipitates were observed, and the reaction proceeded for 1 h. The precipitates were subsequently washed twice with deionized water and finally dried in a vacuum oven at 60 °C for 24 h.

The morphology and size of the nanoparticles were examined by transmission electron microscopy (TEM) (FEI Tecnai G2 20-TEM). TEM samples were prepared by drop-casting a dilute suspension of Fe<sub>3</sub>O<sub>4</sub> nanoparticles in ethanol onto carbon-coated copper grids and drying to remove the ethanol. The functional groups present in the nanoparticles were determined by Fourier transform infrared (FTIR) spectroscopy (PerkinElmer FT-IR), in transmission mode (16 scans, wave-number range 4000–450 cm<sup>-1</sup>) and by Raman spectroscopy (inVia 2 Raman spectrometer), using a 532 nm (green) diode laser with 1200 or 1800 L mm<sup>-1</sup> grating. X-ray diffraction (PANalytical Empyrean) in the 2θ range from 10 to 80 with a scan speed 1°/min and a scan step 0.02° was used to determine the crystal nature of the nanoparticles.

### 2.2. Silane Functionalization and Magnetic Property Measurement of Fe<sub>3</sub>O<sub>4</sub> Nanoparticles

Our synthesized Fe<sub>3</sub>O<sub>4</sub> nanoparticles were functionalized by aminopropyl triethoxysilane (APTES) and 3-(trimethoxysilyl)propyl-methacrylate (TMSPM), purchased from Sigma-Aldrich Pty Ltd. The functionalization was performed by incubating the particles in the desired silane at 10% (v/v) in ethanol overnight under continuous shaking. Functionalized particles were washed twice in deionized water before use. The saturation magnetization of the modified and unmodified particles was measured by a magnetic property measurement system (Quantum Design) at room temperature.

### 2.3. PEGDM Synthesis

PEGDM was synthesized as reported previously.<sup>[38]</sup> Briefly, 10 kDa poly(ethylene glycol) (PEG) (Sigma Aldrich, 25 g, 2.5 mmol) was dissolved in toluene (Chem-Supply Pty Ltd Australia, 125 mL) and dehydrated twice using a rotary evaporator. The PEG was then dissolved in toluene (37.5 mL), dichloromethane (VWR International Pty Ltd, 62.5 mL), and triethylamine (290 mg, 2.85 mmol) to react with 2.2 equivalents of methacrylic anhydride (Sigma-Aldrich, 846 mg, 5.5 mmol) for 48 h with stirring. The reaction was quenched by potassium carbonate (6.25 g) followed by filtration and precipitation of the PEGDM via the addition of diethyl ether (200 mL). The powder was finally vacuum filtered and stored at -20 °C until further use.

### 2.4. Hydrogel Preparation on Glass Coverslips

Hydrogels were prepared by dissolving 10 wt% solution of PEGDM (10 kDa) in deionized water degassing with ultrahigh purity argon for 10 min and adding 1, 3, or 5 wt% of the modified and unmodified particles. Crosslinking of the hydrogel was performed by adding a 10% ammonium persulfate (Chem-Supply Pty Ltd Australia) and pure *N,N,N',N'*-tetramethylethylenediamine (TEMED) (Sigma Aldrich) into PEGDM hydrogel solution in a 5:1:250 ratio, respectively. Drops (20 μL) of gel solution were added onto a hydrophobic glass slide followed by placing a functionalized glass coverslip on top. Glass coverslips were functionalized by first washing with ethanol and DI water and then treating with ethanol, glacial acetic acid, and TMSPM solution in a 46:3:1 ratio for 10 min before air drying. After 1 h, the glass coverslips with the thin layer of hydrogel were gently removed from the glass slide.

Protein (fibronectin) incorporation was carried out by incubating 150 μL fibronectin solution on a planar polydimethylsiloxane (PDMS) stamp surface for 30 min (25 μg mL<sup>-1</sup>) and then removing excess solution from the PDMS stamps surface by gentle airflow. Fibronectin was transferred to the gel surface by stamping with gentle pressure for 1 min. After stamping, the gels were washed twice with DI water and stored in 12-well plate in DI water until cell culture.

### 2.5. Rheology

All rheological measurements were performed using an Anton Paar MCR 302 rheometer with a parallel plate geometry (25 mm Disk, 1 mm measuring distance, 600 μL of prehydrogel solution) at 25 °C. Oscillatory measurements were performed with 0.02% strain and a 1 Hz frequency for the duration of gelation. Shear rate sweeps were performed with a 1 Hz frequency from a shear rate of 0.01–10 (1/s) at a log ramp scale over 4 min.

### 2.6. Cell Culture

Adipose-derived mesenchymal stem cells (ATCC PCS-500-011) (ADSCs) were cultured in low-glucose Dulbecco's modified Eagle's medium (Thermo Fisher Scientific, Cat. No. 11885084) supplemented with 10% (v/v) fetal bovine serum (BOVO-GEN, Australia, Cat. No. SFBS-AU) and 1% (v/v) penicillin and streptomycin (Sigma Aldrich, Cat. No. P4333) at 37 °C, 5% CO<sub>2</sub> in a humidified incubator. The medium was changed every 48 h and cells were passaged at 80–85% confluency. All ADSCs used in the experiments were at the passage from 4 to 10. To compare the ADSC response with and without a magnetic field, permanent magnets (0.23 T) were placed under the 12 well plate during culture. ADSCs were cultured in the PEG gels for 48 h in the presence and absence of a magnetic field before fixing.

### 2.7. Immunofluorescence

Directly after culture in the presence or absence of a magnetic field, cells were fixed with 4% paraformaldehyde (Sigma-Aldrich Pty Ltd.) for 20 min and permeabilized in 0.1% Triton X-100 (Sigma-Aldrich Pty Ltd.) in phosphate buffered saline

(PBS) for 30 min. 1% bovine serum albumin (BSA) was used to block the cells for 15 min.  $\alpha$ -SMA (1:400) labeling was performed in 1% BSA (w/v) in PBS for 1 h at room temperature, followed by rinsing twice with PBS. Secondary antibody labeling was performed in 1% BSA in PBS for 1 h in room temperature in the dark. Actin and nuclei were stained by 488-phalloidin (1:200) and 4,6-diamidino-2-phenylindole (DAPI: 1:4000), respectively. Immunofluorescence microscopy was conducted using a Zeiss LSM 800 confocal microscope. Cell area was measured from phalloidin staining of the actin cytoskeleton by measuring the average cell area of 150 cells using ImageJ.  $\alpha$ -SMA intensity was calculated by measuring raw intensity after background subtraction of cells expressing  $\alpha$ -SMA using Image J. The percentage of cells expressing  $\alpha$ -SMA was quantified by automatic counting of cells expressing  $\alpha$ -SMA above a preset threshold using 3 sets of replicates, 5 fields of view for each replicate, and at least 10 cells per field of view.

### 2.8. Statistical Analysis

Statistically significant differences were determined by one-way analysis of variance (ANOVA) with Tukey's HSD post hoc analysis done for statistical significance. The data were expressed as mean  $\pm$  standard deviation (SD).

## 3. Results and Discussion

### 3.1. Characterization of Fe<sub>3</sub>O<sub>4</sub> Nanoparticle

Iron oxide nanoparticles were synthesized with a chemical coprecipitation method by reacting iron salts with ammonium hydroxide solution in a nitrogen environment.<sup>[36,37]</sup> Figure 1a shows a TEM image of nanoparticles revealing their spherical morphology and narrow size variation with an average particle size of

10.53  $\pm$  1.5 nm (Figure 1b). XRD of the particles clearly shows the presence of crystal planes in  $2\theta$  peaks at 21.4°, 30.2°, 35.5°, 41.5°, 50.6°, 63.2°, and 67.5° (Figure 1c), which are attributed to the characteristic crystal planes 211, 220, 311, 400, 422, 511, and 440 of magnetite.<sup>[39,40]</sup> The Raman spectrum in Figure 1d shows the presence of characteristic peaks of magnetite at 487 and 661 cm<sup>-1</sup>.<sup>[41,42]</sup> Furthermore, FTIR spectrum in Figure 1e shows the presence of Fe–O stretching band of bulk magnetite at 543 and 624 cm<sup>-1</sup>.<sup>[39,43]</sup> Overall, these characterizations demonstrate the successful synthesis of spherical Fe<sub>3</sub>O<sub>4</sub> nanoparticles.

### 3.2. Silane Functionalization of Fe<sub>3</sub>O<sub>4</sub> Nanoparticles

With the desire to covalently stabilize the nanoparticles into a hydrogel system, we functionalized the particles with two silanes: APTES and TMSPM. Here, we hypothesize that the methacrylate groups on the TMSPM particles will covalently crosslink to the dimethacrylate groups on the PEGDM polymers to enable enhanced particle retention. In this case, the APTES will function as a control coating which should not covalently bond to the polymer backbone. FTIR spectrum (Figure 2a) upon treatment with APTES, shows characteristic peaks for chemical conjugation at  $\approx$ 1050 cm<sup>-1</sup>, attributed to open-chain siloxane groups<sup>[13,44]</sup> and the TMSPM-treated particles showing characteristic peaks at  $\approx$ 1638 cm<sup>-1</sup> (C=C) and  $\approx$ 1706 cm<sup>-1</sup> (C=O).<sup>[13,45]</sup> Figure 2b demonstrates the superparamagnetic behavior of the modified and unmodified nanoparticles as there are no observed remanent magnetization and all the hysteresis loops pass through the origin.<sup>[46]</sup> The saturation magnetization of the Fe<sub>3</sub>O<sub>4</sub>, APTES-modified Fe<sub>3</sub>O<sub>4</sub> and TMSPM-modified Fe<sub>3</sub>O<sub>4</sub> were found to be 6.92, 6.43, and 6.41 emu g<sup>-1</sup>, respectively, which indicates little reduction (7%) in saturation magnetization after silane functionalization.

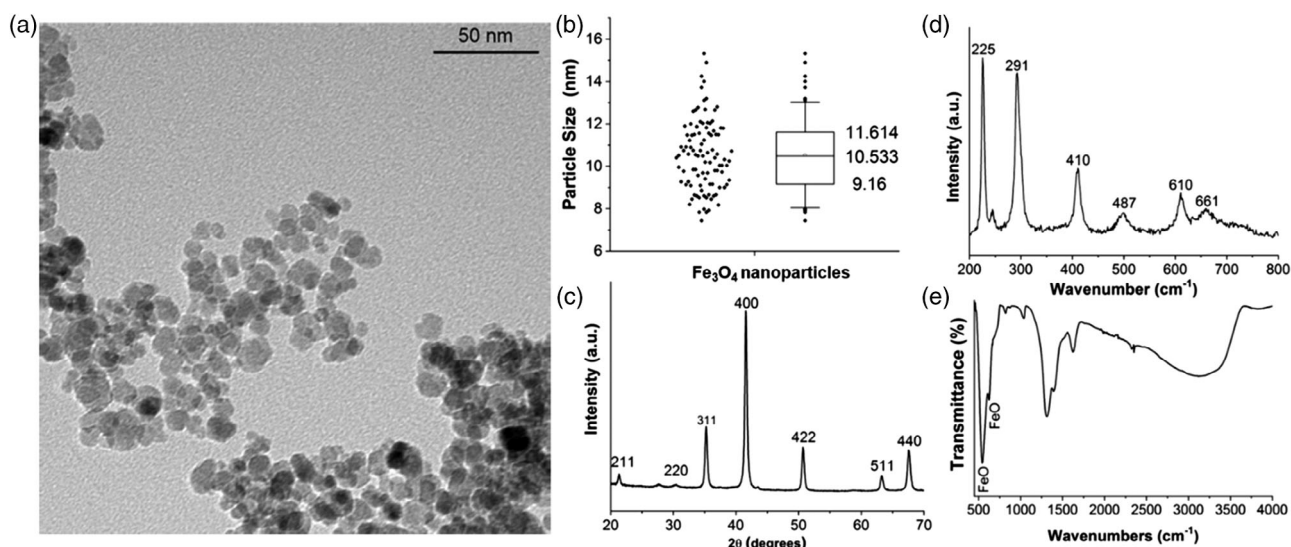


**Figure 1.** Characterization of Fe<sub>3</sub>O<sub>4</sub> nanoparticles: a) TEM image of spherical nanoparticles, b) Quantification of average particle size (10.53  $\pm$  1.5 nm) from TEM images, c) XRD pattern with characteristic crystal plane peaks of magnetite, d) Raman spectrum with the characteristic peaks of magnetite, and e) FTIR spectrum of Fe<sub>3</sub>O<sub>4</sub> nanoparticles with FeO stretching bands at 543 and 624 cm<sup>-1</sup>.

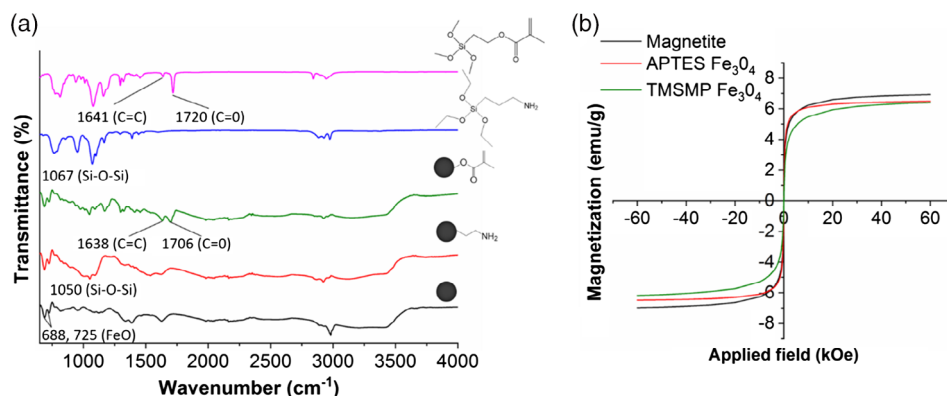


**Figure 2.** a) FTIR analysis of synthesized nanoparticles, functionalized nanoparticles, APTES and TMSPM neat chemicals; colored lines (black, red, green, blue, and pink) represent FTIR spectrum of magnetite, APTES-modified magnetite, TMSPM-modified magnetite, APTES, and TMSPM, respectively, and b) magnetic hysteresis loop of modified and unmodified magnetite nanoparticles show the superparamagnetic behavior.

### 3.3. Nanoparticle Integration into Hydrogels and Rheological Analysis

Magnetic nanoparticle hydrogel composites are promising materials for changing mechanical properties in response to external fields.<sup>[47,48]</sup> PEG-based hydrogels are widely used materials for cell culture and tissue engineering due to biocompatibility, tunable stiffness, and the ability to incorporate versatile functional groups.<sup>[49,50]</sup> In an effort to use PEG as a matrix for the inclusion of iron oxide materials, we tried direct mixing of 10 kDa PEG-DM with our pristine and silanized particles. Changes in the storage ( $G'$ : black) and loss ( $G''$ : red) modulus after initiating radical crosslinking for PEG-DM gels in the presence of nanoparticles (unmodified and modified) over time can be seen in **Figure 3**. A sudden increase in  $G'$  was observed in all samples within the first minute indicating the onset of crosslinking. After 3 min,  $G'$  reached a plateau in all samples. All samples tested show comparable final storage moduli, indicating no significant difference between particles with different surface coatings (all storage moduli are within 3% of each other). It was noted, however, that the presence of particles led to a slight decrease in polymerization kinetics and final modulus, suggesting that particle inclusion impedes the network formation. Surprisingly, integrating particles with pendant methacryloyl moieties did not change the bulk rheology of the gel with no magnetic field applied.

Next, we asked whether there would be variation in particle retention within the hydrogels over time. Considering the nanoscale size of the  $\text{Fe}_3\text{O}_4$  in contrast to the microscale meshwork of the radical polymerized PEG gels (average pore size ranges between 5 to 70  $\mu\text{m}$ ),<sup>[51,52]</sup> we expected easy diffusion of the nanoparticles out of the hydrogel. However, when subjected to a magnetic field up to 48 h followed by centrifugation of the media, no evidence of particle release from the hydrogels was found and there was no difference between the surface coatings. This result is somewhat surprising considering the small particle size to the mesh size. However, previous work has demonstrated strong adhesion between nanoparticles and polymer chains that can promote retention.<sup>[53,54]</sup> Therefore, for subsequent cell culture experiments unmodified nanoparticles were used.

### 3.4. Variations in Cell Morphology with Nanoparticle Content and Magnetic Fields

The mechanical characteristics of cell culture substrates, including stiffness and topography, will influence cell spreading.<sup>[30,55,56]</sup> Our previous work has demonstrated how a nearly three orders of magnitude increase in the storage modulus can be achieved by the application of a magnetic field to align micrometre scale carbonyl iron particles incorporated into a polyacrylamide hydrogel composite.<sup>[13]</sup> Furthermore, that study showed how the magnetic field-induced stiffening could be used to dynamically modulate MSC osteogenesis.<sup>[13]</sup> Thus, we reasoned that magnetic fields applied to our nanoparticle composite PEG-based hydrogels would influence the particle organization, thereby impacting the interconnected mesh network and the cell perceived stiffness. Furthermore, while magnetic properties of nanoparticle composites do not generally show a discontinuity in properties at the percolation threshold, the storage modulus generally does and nanoparticles offer a much lower percolation threshold compared to micrometer scale particles.<sup>[57–60]</sup> Thus, the nanoscale particles used in the present study should demonstrate a beneficial stiffening effect at much lower volume fractions than the 30 vol% used in our previous work.<sup>[13]</sup>

Adipose-derived stem cells (ADSC) were cultured at 1970 cells  $\text{cm}^{-2}$  for 48 h followed by immunostaining for nuclei and filamentous actin. It can be seen from **Figure 4b** that, nanoparticle incorporation does not influence cell area up to 3 wt%; however, incorporation of 5 wt%  $\text{Fe}_3\text{O}_4$  nanoparticles leads to an increase of  $\approx 40\%$  in average cell area (2862–4012  $\mu\text{m}^2$ ) without applied fields. This result suggests that the incorporation of particles at higher weight fraction exceeds the percolation threshold and leads to an increase in the cell-perceived stiffness of the hydrogel. Although shear rheology showed a difference in the modulus no greater than 3% as particle content increases, it is important to note that the percolation threshold not only depends on the particle size but also on the architecture of the particle network that is formed (random vs ordered, 2D vs 3D, etc.), which is likely to be quite different during the shear rheometer test. Nonetheless, other factors may also be



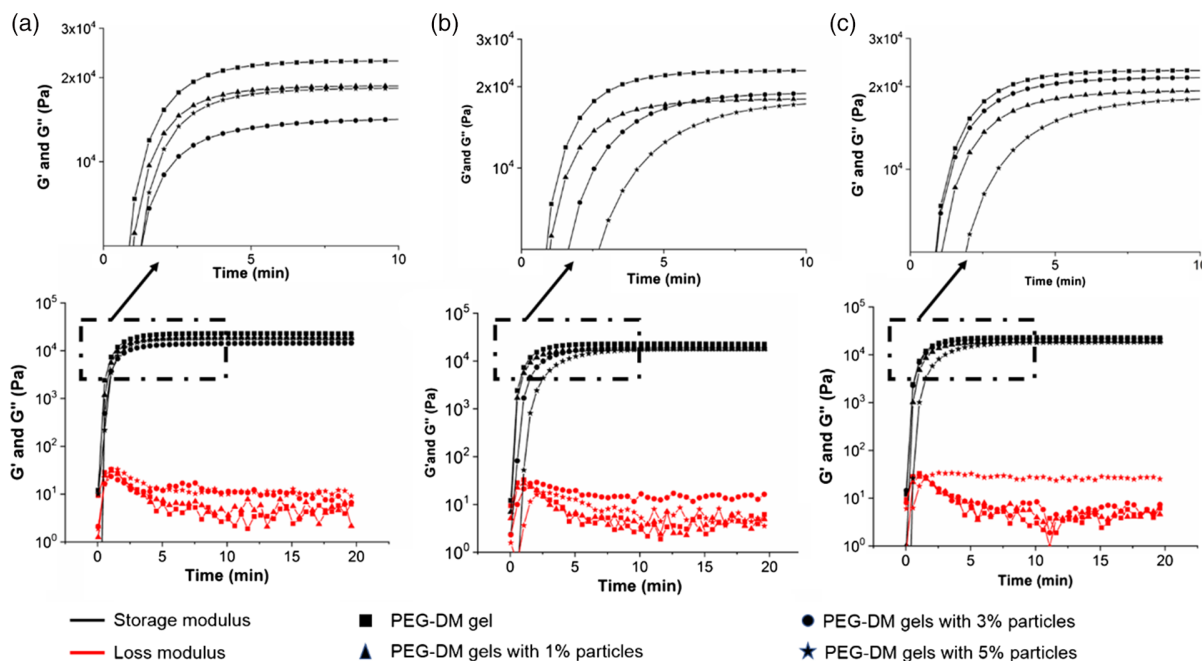


**Figure 3.** Rheological analysis of PEG-DM gels. Amplitude time sweep tests (1 Hz, 0.2% strain) were performed on pure PEG-DM and 1, 3, and 5 wt% of a)  $\text{Fe}_3\text{O}_4$ , b) APTES-modified  $\text{Fe}_3\text{O}_4$ , and c) TMSPM-modified  $\text{Fe}_3\text{O}_4$  nanoparticles.

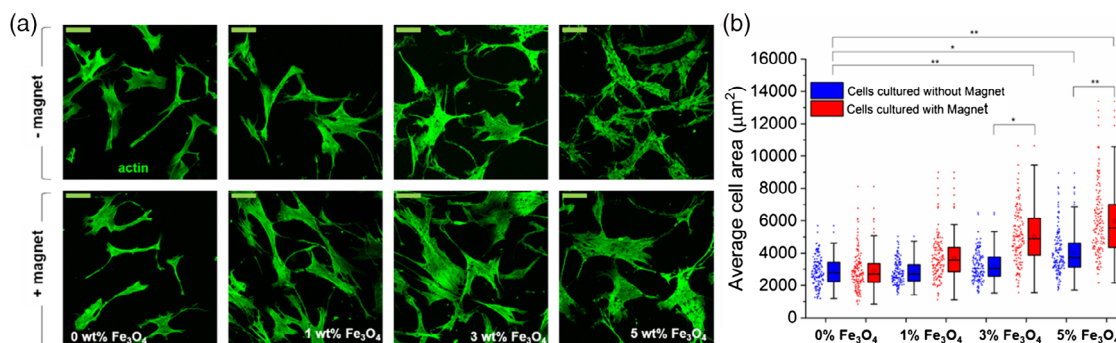


**Figure 4.** a) Representative images of ADSCs cultured in the presence and absence of magnets stained for filamentous actin (scale bar = 100  $\mu\text{m}$ ) and b) quantification of average cell area ( $n = 150$ , number of cells).

responsible for the cell response at 5 wt%. Previous studies of cell adhesion to nanomaterial-impregnated hydrogels demonstrate that ECM matrix roughness contributed to cell spreading.<sup>[61,62]</sup> Therefore, we also speculate that at high particle content, cells may increase their spreading on account of interfacial particle density. In contrast, when the composite gels were exposed to a magnetic field, using a permanent magnet at 0.83 mm from the gel to provide a field of 0.23 T, cells adherent to hydrogels containing 3 and 5 wt%  $\text{Fe}_3\text{O}_4$  nanoparticles showed a significant increase in cell area of 74% and 107%, respectively, with considerable variability across the population.

This strong cell response is consistent with a magnetic field-induced stiffening of the hydrogel composite.<sup>[13]</sup> To establish the relationship between substrate stiffness and cell area, we compared the cell area when adherent to PEG hydrogels spanning 5–100 kPa (Figure 1, Supporting Information).

Interpolation from our starting hydrogel of 5 kPa stiffness, cell area changes indicate that our material is stiffened by magnetic fields to  $\approx 41$  kPa (1 wt%  $\text{Fe}_3\text{O}_4$ ), 73 kPa (3 wt%  $\text{Fe}_3\text{O}_4$ ), and 97 kPa (5 wt%  $\text{Fe}_3\text{O}_4$ ). Together these results show how integrating magnetic  $\text{Fe}_3\text{O}_4$  nanoparticles into PEG-based hydrogels will lead to a change in the perceived mechanical properties at the interface spanning a wide range of stiffness. There are several potential mechanisms for magnetic field-induced stiffening: 1) applied magnetic fields lead to alignment of the particles, thereby presenting a more rigid composite material to the adherent cells, and 2) physical interaction of particles directly with polymer segments leads to a material where the meshwork stretches under applied magnetic fields. In previous studies using carbonyl iron microparticles, the former mechanism is believed to cause stiffening.<sup>[13]</sup> In the current study, the observation that the particles remain integrated with the gel under

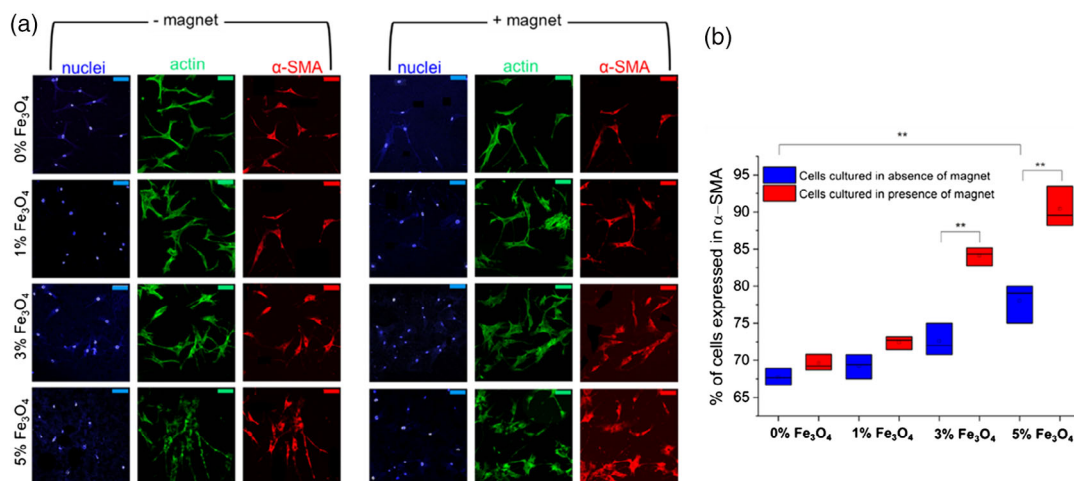


**Figure 5.** a) Representative images of ADSCs cultured in the presence and absence of magnets (scale bar = 100 μm) and b) quantification of α-SMA expression ( $n = 3$ , replicate hydrogel).

applied force supports the latter mechanism. It is likely that a combination of these mechanisms is involved to facilitate stiffening under a magnetic field. However, discerning the precise mechanism is challenging at the nanoscale and will require new instrumentation for advanced imaging that is not currently available.

### 3.5. Magnetic Stiffening to Direct Stem-Cell Differentiation

There is considerable evidence that cell phenotype and propensity to differentiate are directly linked to the adhesive microenvironment and the ability of cells to change shape and area.<sup>[2,27,63]</sup> An important cell type for guiding the form and function of tissues and maintaining the integrity of membranes in tissue and vasculature is the myofibroblast. Tissue engineering requires this cell type to be readily available for integration with tissue-specific cells, which has led to the need for rapid and simple isolation and differentiation protocols. ADSCs have been shown to undergo a fibroblast-to-myofibroblast transition on account of the mechanical microenvironment.<sup>[27]</sup> One aspect of myofibroblast differentiation is a change in cell shape as they become more contractile, leading to expression of smooth muscle actin (α-SMA). As our magnetic stiffening of the substrate influences the adhesive areas of ADSCs, we asked whether this change in shape is linked to the propensity to undergo smooth muscle myogenesis. ADSCs were cultured on PEG-Fe<sub>3</sub>O<sub>4</sub> composite hydrogels at 0, 1, 3, and 5 wt% nanoparticle content with and without magnetic fields. Interestingly, while the change in area was modest as nanoparticle content increased, we see a consistent increase in the fraction of cells expressing α-SMA, suggesting that increasing particles at the interface influences the myofibroblast phenotype (Figure 5a). Attenuating a magnetic field over two days leads to an additional increase in cells expressing α-SMA, even for the control condition where nanoparticles are not present. The presence of a magnetic field for ADSCs cultured in gels with 3 and 5 wt% Fe<sub>3</sub>O<sub>4</sub> nanoparticles show a significant increase in α-SMA compared to without a magnetic field (84.1%

compared to 72.6% in gels with 3 wt% Fe<sub>3</sub>O<sub>4</sub> and 90% compared to 78% in gels with 5 wt% Fe<sub>3</sub>O<sub>4</sub>, respectively; Figure 5b). We also measured the intensity of the cells expressed in α-SMA and found an increase in intensity when cultured in the presence of a magnetic field (Figure 2, Supporting Information). The myofibroblast phenotype can be determined through binary analysis; that is, positive versus negative expression of α-SMA.<sup>[56]</sup> An increase in α-SMA expression will indicate enhanced contractility within the population. Therefore, in this study, we see that stiffening through applied magnetic fields will influence both the process of myofibrillogenesis (% expression) and the degree of myofibroblast contraction (intensity).

## 4. Conclusion

Matrix stiffening on account of cell-matrix engagement, with a view to influencing cell activity such as spreading and lineage specification, is a well-explored technique for manipulating phenotype and behavior in the laboratory. Our study demonstrates a simple approach to modulate ADSC adhesive characteristics through attenuation of a magnetic field using permanent magnets in cell culture. Stiffening of magnetic nanoparticle hydrogel composites leads to a significant increase in cell area and subsequent enrichment of the fraction expressing α-SMA. As a reversible technique, this platform may prove useful to scientists exploring the dynamics of matrix stiffening with broad applicability to many adherent cell systems. Furthermore, enriching a desired cell type in culture could be leveraged toward the production of therapeutically useful cells, in this case myofibroblasts, that may then be harvested for direct use or for incorporation into tissue-engineered scaffolds.

## Supporting Information

Supporting Information is available from the Wiley Online Library or from the author.

## Acknowledgements

This work was supported through funding from the Australian Research Council Grant FT180100417. The authors acknowledge the help and support of staff at the Biomedical Imaging Facility and the Biological Specimen Preparation Laboratory of the UNSW Mark Wainwright Analytical Center.

## Conflict of Interest

The authors declare no conflict of interest.

## Data Availability Statement

Research data are not shared.

## Keywords

adipose-derived stromal cells, differentiation, hydrogels, magnetoactive, nanoparticle, smooth muscles

Received: November 6, 2020

Revised: January 13, 2021

Published online:

- [1] M. S. J. S. Steinberg, *Reconstru. Tissues Dissoc. Cells* **1963**, 141, 401.
- [2] K. H. Vining, D. J. Mooney, *Nat. Rev. Mol. Cell Biol.* **2017**, 18, 728.
- [3] D. E. Ingber, *FASEB J.* **2006**, 20, 811.
- [4] N. Wang, J. P. Butler, D. E. J. S. Ingber, *Science* **1993**, 260, 1124.
- [5] F. M. Fumasi, N. Stephanopoulos, J. L. Holloway, *J. Appl. Polym. Sci.* **2020**, 137, 49058.
- [6] A. M. Kloxin, A. M. Kasko, C. N. Salinas, K. S. Anseth, *Science* **2009**, 324, 59.
- [7] R. S. Stowers, S. C. Allen, L. J. Suggs, *Proc. Natl. Acad. Sci.* **2015**, 112, 1953.
- [8] J. I. Edahiro, K. Sumaru, Y. Tada, K. Ohi, T. Takagi, M. Kameda, T. Shinbo, T. Kanamori, Y. Yoshimi, *Biomacromolecules* **2005**, 6, 970.
- [9] N. Yamada, T. Okano, H. Sakai, F. Karikusa, Y. Sawasaki, Y. Sakurai, *Die Makromol. Chem., Rapid Commun.* **1990**, 11, 571.
- [10] X. Zhu, J. DeGraaf, F. M. Winnik, D. Leckband, *Langmuir* **2004**, 20, 1459.
- [11] M. Panayiotou, R. J. P. Freitag, *Polymer* **2005**, 46, 6777.
- [12] C. S. Kwok, P. D. Mourad, L. A. Crum, B. D. Ratner, *J. Biomed. Mater. Res.* **2001**, 57, 151.
- [13] A. A. Abdeen, J. Lee, N. A. Bharadwaj, R. H. Ewoldt, K. A. Kilian, *Adv. Healthcare Mater.* **2016**, 5, 2536.
- [14] S. Bell, A.-L. Redmann, E. M. Terentjev, *Biophys. J.* **2019**, 116, 551.
- [15] D. E. Discher, P. Janmey, Y.-L. Wang, *Science* **2005**, 310, 1139.
- [16] T. Yeung, P. C. Georges, L. A. Flanagan, B. Marg, M. Ortiz, M. Funaki, N. Zahir, W. Ming, V. Weaver, P. A. Janmey, *Cell Motility Cytoskeleton* **2005**, 60, 24.
- [17] C. Lee, A. Grodzinsky, M. J. B. Spector, *Biomaterials* **2001**, 22, 3145.
- [18] J. D. Mih, A. Marinkovic, F. Liu, A. S. Sharif, D. J. Tschumperlin, *J. Cell Sci.* **2012**, 125, 5974.
- [19] P. P. Provenzano, P. J. Keely, *J. Cell Sci.* **2011**, 124, 1195.
- [20] N. D. Evans, C. Minelli, E. Gentleman, V. LaPointe, S. N. Patankar, M. Kallivretaki, X. Chen, C. J. Roberts, M. M. Stevens, *Eur. Cell Mater.* **2009**, 18, e13.
- [21] A. S. Mao, J.-W. Shin, D. J. B. Mooney, *Biomaterials* **2016**, 98, 184.
- [22] J. S. Park, J. S. Chu, A. D. Tsou, R. Diop, Z. Tang, A. Wang, S. Li, *Biomaterials* **2011**, 32, 3921.
- [23] A. Desmoulière, C. Chaponnier, G. Gabbiani, *Wound Repair Regener.* **2005**, 13, 7.
- [24] G. Gabbiani, *J. Pathol.* **2003**, 200, 500.
- [25] W. Gu, X. Hong, A. Le Bras, W. N. Nowak, S. I. Bhaloo, J. Deng, Y. Xie, Y. Hu, X. Z. Ruan, Q. Xu, *J. Biol. Chem.* **2018**, 293, 8089.
- [26] M. Rabbani, M. Tafazzoli-Shadpour, M. A. Shokrgozar, M. Janmaleki, M. Teymoori, *Tissue Eng. Regener. Med.* **2017**, 14, 279.
- [27] M. Rothdiener, M. Hegemann, T. Uynuk-Ool, B. Walters, P. Papugy, P. Nguyen, V. Claus, T. Seeger, U. Stoeckle, K. A. Boehme, W. K. Aicher, *Sci. Rep.* **2016**, 6, 35840.
- [28] R. McBeath, D. M. Pirone, C. M. Nelson, K. Bhadriraju, C. S. Chen, *Dev. Cell* **2004**, 6, 483.
- [29] D. Zhang, K. A. Kilian, *Biomaterials* **2013**, 34, 3962.
- [30] J. Lee, A. A. Abdeen, D. Zhang, K. A. Kilian, *Biomaterials* **2013**, 34, 8140.
- [31] D. Zhang, K. A. Kilian, *J. Mater. Chem. B* **2014**, 2, 4280.
- [32] Z. Gong, L. E. Niklason, *FASEB J.* **2008**, 22, 1635.
- [33] M. Hellstrom, P. Lindahl, A. Abramsson, C. Betsholtz, *Development* **1999**, 126, 3047.
- [34] N. Kobayashi, T. Yasu, H. Ueba, M. Sata, S. Hashimoto, M. Kuroki, M. Saito, M. Kawakami, *Exp. Hematol.* **2004**, 32, 1238.
- [35] K. Kurpinski, J. Chu, C. Hashi, S. Li, *Proc. Natl. Acad. Sci.* **2006**, 103, 16095.
- [36] K. Petcharoen, A. Sirivat, *Mater. Sci. Eng., B* **2012**, 177, 421.
- [37] Y. S. Kang, S. Risbud, J. F. Rabolt, P. Stroeve, *Chem. Mater.* **1996**, 8, 2209.
- [38] T. G. Molley, X. Wang, T. T. Hung, P. B. Jayathilaka, J. L. Yang, K. A. Kilian, *Adv. Biosyst.* **2020**, 4, 2000056.
- [39] N. M. Salem, A. L. Ahmad, A. M. Awwad, *Nanosci. Nanotechnol.* **2013**, 3, 48.
- [40] Z. Takai, M. K. Mustafa, S. Asman, A. Sekak, *J. Human Dev. Commun.* **2019**, 12, 37.
- [41] M. Hanesch, *Geophys. J. Int.* **2009**, 177, 941.
- [42] D. De Faria, S. Venâncio Silva, M. J. De Oliveira, *J. Raman Spectrosc.* **1997**, 28, 873.
- [43] O. M. Lemine, K. Omri, B. Zhang, L. El Mir, M. Sajjeddine, A. Alyamani, M. Bououdina, *Superlattices Microstruct.* **2012**, 52, 793.
- [44] M. Yamaura, R. L. Camilo, L. C. Sampaio, M. A. Macedo, M. Nakamura, H. E. Toma, *J. Magn. Magn. Mater.* **2004**, 279, 210.
- [45] D. Lin-Vien, N. B. Colthup, W. G. Fateley, J. G. Grasselli, *The Handbook of Infrared and Raman Characteristic Frequencies of Organic Molecules*, Elsevier, Amsterdam/New York **1991**.
- [46] S. Aktaş, *Doctoral dissertation*, University of Leicester **2014**.
- [47] Z. Liu, J. Liu, X. Cui, X. Wang, L. Zhang, P. Tang, *Front. Chem.* **2020**, 8, 124.
- [48] Y. Wang, B. Li, F. Xu, Z. Han, D. Wei, D. Jia, Y. Zhou, *Biomacromolecules* **2018**, 19, 3351.
- [49] A. Escudero-Castellanos, B. E. Ocampo-García, M. V. Domínguez-García, J. Flores-Estrada, M. V. Flores-Merino, *J. Mater. Sci.: Mater. Med.* **2016**, 27, 176.
- [50] J. J. B. Zhu, *Biomaterials* **2010**, 31, 4639.
- [51] M. Jamadi, P. Shokrollahi, B. Houshmand, M. D. Joupari, F. Mashhadiabbas, A. Khademhosseini, N. Annabi, *Macromol. Biosci.* **2017**, 17, 1600479.
- [52] H. H. Barnett, A. M. Heimbeck, I. Pursell, R. A. Hegab, B. J. Sawyer, J. J. Newman, M. E. Caldorera-Moore, *J. Biomater. Sci., Polym. Ed.* **2019**, 30, 895.
- [53] Y. Sapir, S. Cohen, G. Friedman, B. Polyak, *Biomaterials* **2012**, 33, 4100.
- [54] Y. Li, G. Huang, X. Zhang, B. Li, Y. Chen, T. Lu, T. J. Lu, F. Xu, *Adv. Funct. Mater.* **2013**, 23, 660.
- [55] R. G. Breuls, T. U. Jiya, T. H. Smit, *Open Orthop. J.* **2008**, 2, 103.
- [56] D. Zhang, M. B. Sun, J. Lee, A. A. Abdeen, K. A. Kilian, *J. Biomed. Mater. Res. Part A* **2016**, 104, 1212.

- [57] L. C. Costa, M. Valente, M. A. Sa, F. Henry, *Polym. Bull.* **2006**, *57*, 881.
- [58] D. Y. Godovski, *Thermal and Electrical Conductivity of Polymer Materials*, Springer Berlin Heidelberg, Berlin, Heidelberg **1995**, pp. 79–122.
- [59] J. Zhu, S. Wei, Y. Li, L. Sun, N. Haldolaarachchige, D. P. Young, C. Southworth, A. Khasanov, Z. Luo, Z. Guo, *Macromolecules* **2011**, *44*, 4382.
- [60] T. Mitsumata, T. Hachiya, K. Nitta, *Eur. Polym. J.* **2008**, *44*, 2574.
- [61] J. Y. Lim, J. C. Hansen, C. A. Siedlecki, J. Runt, H. J. Donahue, *J. R. Soc. Interface* **2005**, *2*, 97.
- [62] H.-I. Chang, Y. Wang, in *Regenerative Medicine and Tissue Engineering-Cells and Biomaterials*, InTechOpen, Rijeka, Croatia **2011**, pp. 569–588.
- [63] U. S. Schwarz, S. A. Safran, *Phys. Adherent Cells* **2013**, *85*, 1327.